

Article

# Chiral Selectors in Voltammetric Sensors Based on Mixed Phenylalanine/Alanine Cu(II) and Zn(II) Complexes

Rufina A. Zilberg <sup>\*</sup>, Tatyana V. Berestova <sup>\*</sup>, Ruslan R. Gizatov, Yulia B. Teres, Miras N. Galimov and Elena O. Bulysheva

Department of Chemistry, Bashkir State University, 450000 Ufa, Russia

<sup>\*</sup> Correspondence: zilbergra@yandex.ru (R.A.Z.); berestovatv@gmail.com (T.V.B.)

**Abstract:** A practical application composite based on mixed chelate complexes  $[M(S-Ala)_2(H_2O)_n]-[M(S-Phe)_2(H_2O)_n]$  ( $M = Cu(II), Zn(II); n = 0-1$ ) as chiral selectors in enantioselective voltammetric sensors was suggested. The structures of the resulting complexes were studied by XRD, ESI-MS, and IR- and NMR-spectroscopy methods. It was determined that enantioselectivity depends on the metal nature and on the structure of the mixed complex. The mixed complexes, which were suggested to be chiral selectors, were stable under the experimental conditions and provided greater enantioselectivity in the determination of chiral analytes, such as naproxen and propranolol, in comparison with the amino acids they comprise. The best results shown by the mixed copper complex  $[Cu(S-Ala)_2]-[Cu(S-Phe)_2]$  were:  $i_{pS}/i_{pR} = 1.27$  and  $\Delta E_p = 30$  mV for Nap; and  $i_{pS}/i_{pR} = 1.37$  and  $\Delta E_p = 20$  mV for Prp. The electrochemical and analytical characteristics of the sensors and conditions of voltammogram recordings were studied by differential pulse voltammetry. Linear relationships between the anodic current and the concentrations of Nap and Prp enantiomers were achieved in the range of  $2.5 \times 10^{-5}$  to  $1.0 \times 10^{-3}$  mol L<sup>-1</sup> for GCE/PEC- $[Cu(S-Ala)_2]-[Cu(S-Phe)_2]$  and  $5.0 \times 10^{-5}$  to  $1.0 \times 10^{-3}$  for GCE/PEC- $[Zn(S-Ala)_2(H_2O)]-[Zn(S-Phe)_2(H_2O)]$ , with detection limits (3 s/m) of 0.30–1.24  $\mu$ M. The suggested sensor was used to analyze Nap and Prp enantiomers in urine and plasma samples.

**Keywords:** voltammetry; enantioselective sensors; mixed chelate complexes of Cu(II) and Zn(II); S-alanine; S-phenylalanine; naproxen enantiomers; propranolol enantiomers



**Citation:** Zilberg, R.A.; Berestova, T.V.; Gizatov, R.R.; Teres, Y.B.; Galimov, M.N.; Bulysheva, E.O. Chiral Selectors in Voltammetric Sensors Based on Mixed Phenylalanine/Alanine Cu(II) and Zn(II) Complexes. *Inorganics* **2022**, *10*, 117. <https://doi.org/10.3390/inorganics10080117>

Academic Editors: Izilda Aparecida Bagatin and Fábio Ruiz Simões

Received: 19 July 2022

Accepted: 9 August 2022

Published: 12 August 2022

**Publisher's Note:** MDPI stays neutral with regard to jurisdictional claims in published maps and institutional affiliations.



**Copyright:** © 2022 by the authors. Licensee MDPI, Basel, Switzerland. This article is an open access article distributed under the terms and conditions of the Creative Commons Attribution (CC BY) license (<https://creativecommons.org/licenses/by/4.0/>).

## 1. Introduction

Enantioselective voltammetric sensors (EVS) significantly expand the capabilities of electrochemical analysis and enable the analysis of optically active compounds [1–5], which is very important in pharmaceuticals and medicine [6,7]. Thus, the development of enantioselective sensors makes it possible to create inexpensive and affordable portable systems for the quality control of modern pharmaceuticals and dietary supplements without preliminary sample preparation and to analyze the contents of active components of pharmaceuticals in biological fluids.

The existing EVS can be separated into two large groups based on the production method [2]. The first group includes sensors that transfer the surface chirality directly to the sensor, for example, by molecular imprinting (MIP) [8–10]. Rather recently, by analogy with MIP polymers, EVS based on chiral mesoporous metals obtained by electrodeposition of Au, Ag, Pt, Pd, Ni, etc., on inert electrodes in the presence of chiral electroactive templates were suggested [11–13]. The drawbacks of MIP sensors include the lack of versatility and the difficulty of removing template molecules.

The second group includes sensors from achiral materials, while the chirality of the sensor surface is achieved by introducing a chiral selector into the sensor [14–26]. A composite sensors can have a “film” structure if a chiral selector is applied onto the working

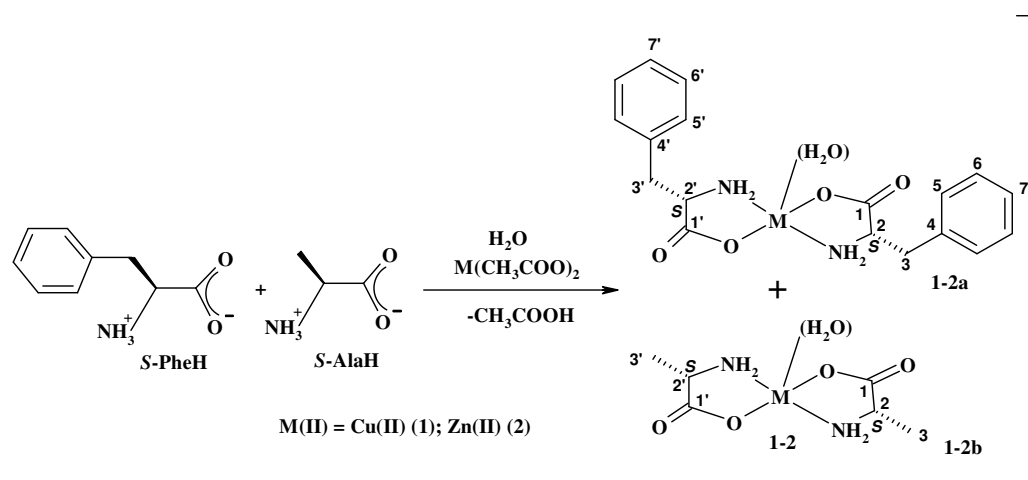
electrode surface or it can be a paste into which a chiral selector is incorporated in a required amount [14–21].

Currently, chiral selectors are mainly made of optically active organic compounds. Therefore, the majority of the known or synthesized chiral compounds is comprised of organic molecules or organic polymers with very diverse structures. Undoubtedly, such a variety of optically active organic compounds makes it possible to select a chiral selector with the necessary parameters for almost any task. However, the difficulty of synthesizing chiral compounds with a required optical purity considerably limits the range of available composite sensors. Due to the peculiarities of the atomic and electronic structure, the variety of optically active inorganic compounds is much smaller, and most of them are not applicable for the replacement of organic chiral selectors. However, advances in the chemistry of coordination compounds, transition metal complexes in particular, make it possible to obtain readily available optically active complexes whose enantioselectivity depends on the nature of the metal and on the structure of the complex and of the chiral ligands. The use of available organic ligands of natural origin, for example,  $\alpha$ -amino acids, provides vast possibilities for making a wide range of chiral selectors [17,27,28] whose enantioselectivity and other electrochemical parameters can be controlled by the structure of the radical of the  $\alpha$ -amino acid as the ligand. Of the chelate complexes of transition metals used as chiral selectors, the complexes with phenyl-containing ligands that exhibit efficient enantioselective properties [17,27] are of particular interest. Moreover, they are also alternatives to antibiotics [29] and DNA binding agents [30]. In addition, the development of composites based on mixtures of various chiral components, which make it possible to increase the selectivity of chiral sensors, is also an urgent task.

In view of this, the purpose of our study was to design and synthesize mixed chelate phenyl-containing compounds, namely,  $[\text{Cu}(\text{S-Ala})_2]\text{-}[\text{Cu}(\text{S-Phe})_2]$  (1) and  $[\text{Zn}(\text{S-Ala})_2(\text{H}_2\text{O})]\text{-}[\text{Zn}(\text{S-Phe})_2(\text{H}_2\text{O})]$  (2), and to study the possibility of using these composites as chiral selectors in EVS.

## 2. Results and Discussion

The mixed chelate composites  $[\text{Cu}(\text{S-Ala})_2]\text{-}[\text{Cu}(\text{S-Phe})_2]$  (1) and  $[\text{Zn}(\text{S-Ala})_2(\text{H}_2\text{O})]\text{-}[\text{Zn}(\text{S-Phe})_2(\text{H}_2\text{O})]$  (2) were synthesized using *S*-phenylalanine, *S*-alanine as ligand [31,32], and  $\text{M}(\text{CH}_3\text{COO})_2$  ( $\text{M} = \text{Cu}(\text{II}), \text{Zn}(\text{II})$ ) (Scheme 1). The components were used in a ratio of 1:1:1. The yields of compounds  $[\text{Cu}(\text{S-Ala})_2]\text{-}[\text{Cu}(\text{S-Phe})_2]$  (1) and  $[\text{Zn}(\text{S-Ala})_2(\text{H}_2\text{O})]\text{-}[\text{Zn}(\text{S-Phe})_2(\text{H}_2\text{O})]$  (2) were 48–51%. Complexes **1,2a,b** were characterized by ESI-MS, XRD and IR- spectroscopy methods. NMR-spectroscopy method was used to analysis of the composite **2**.



**Scheme 1.** The synthesis of mixed chelate composites  $[\text{Cu}(\text{S-Ala})_2]\text{-}[\text{Cu}(\text{S-Phe})_2]$  (1) and  $[\text{Zn}(\text{S-Ala})_2(\text{H}_2\text{O})]\text{-}[\text{Zn}(\text{S-Phe})_2(\text{H}_2\text{O})]$  (2).

It was shown that mixed-ligand complexes with the composition  $[M(S\text{-Phe})(S\text{-Ala})(\text{H}_2\text{O})_n]$  ( $M = \text{Cu(II)}, \text{Zn(II)}$ ;  $n = 0\text{--}1$ ) were not formed in the reaction mixture under these conditions. Composites **1,2** were analyzed by the ESI-MS method both in the positive and negative ion modes. According to ESI-MS, mixtures of complexes  $[\text{Cu}(S\text{-Ala})_2]$  (**1a**),  $[\text{Cu}(S\text{-Phe})_2]$  (**1b**), and  $[\text{Zn}(S\text{-Ala})_2(\text{H}_2\text{O})]$ , (**2a**)  $[\text{Zn}(S\text{-Phe})_2(\text{H}_2\text{O})]$  (**2b**) in the ratio of 1:1 were formed (Scheme 1). This may have been due to the hydrophobicity of *S*-phenylalanine and the different solubility and affinity of phenyl-containing complexes **1,2a,b**. Thus, according to ESI-MS, the fragments  $[\text{Cu}(\text{Ala})_2+\text{H}]^+$  (**1a**) 240 *m/z* (239) and  $[\text{Cu}_2(\text{Phe})_2+\text{H}]^+$  were observed in the reaction mixture (**1b**), 456 *m/z* (455). The formation of  $[\text{Cu}_2(\text{Phe})_2+\text{H}]^+$  particles can be caused by the tendency to form associates of bis-*S*-phenylalaninate with an increase in the concentration in solution. This result indicated that complex copper compounds with a coordination number of 4, which corresponded to the square planar configuration of copper amino acid complexes and is consistent with the literature data, were predominantly formed in the solution [31,32]. Therefore, the composition of composite 1 could be expressed by the formula  $[\text{Cu}(S\text{-Ala})_2]\text{--}[\text{Cu}(S\text{-Phe})_2]$ .

In the reaction mixture of composite **2**, the  $[\text{Zn}(\text{Ala})_2\text{--H}]^-$  fragments (**2a**) 240 *m/z* (241) were formed, as well as other particles, for example,  $[\text{Zn}(\text{Ala})_2(\text{Ac})\text{--H}]^-$  (**2a**) 299 *m/z* (300) and  $[\text{Zn}(\text{Phe})_3\text{--H}]^-$  (**2b**) 556 *m/z* (557) in the negative ion mode. At the same time, in the positive ion mode, composite **2** produced the fragments  $[\text{Zn}(\text{Ala})_2+\text{H}]^+$  (**2a**) 242 *m/z* (241) and  $[\text{Zn}(\text{Phe})_3+\text{H}]^+$  (**2b**) 558 *m/z* (557) (Supplementary Materials). Thus, in this case Zn(II) exhibited a coordination number of 5 and had a pyramidal structure in accordance with the literature [33,34] for complexes **2a,b**. According to X-ray diffraction data [33–36] and quantum chemical simulation of the complexes  $[\text{Cu}(S\text{-Phe})_2]$  (**1a**),  $[\text{Cu}(S\text{-Ala})_2]$  (**1b**),  $[\text{Zn}(S\text{-Phe})_2(\text{H}_2\text{O})]$  (**2a**), and  $[\text{Zn}(S\text{-Ala})_2(\text{H}_2\text{O})]$  (**2b**), all the complexes were *trans*-isomers in the *ta-te* [31,37] conformation (Supplementary Materials).

The  $^1\text{H}$  and  $^{13}\text{C}$  NMR spectral data confirmed the structure of complexes **2a,b** in composite **2**. Thus, the protons of the methylene fragment of phenylalanine and the protons at the chiral centers ( $^2\text{C}$ ) shifted to the field relative to the initial ligands, which indicates the coordination of the ligands to the Zn(II) ion. In particular, for phenylalanine, protons of the *CHH* group were observed at 3.11 and 3.27 ppm, and those of *CH* at 4.02 ppm. For complex **2a**, protons of the *CHH* group were observed at 3.02 and 3.23 ppm, and those of *CH* at 3.79 ppm. At the same time, the protons of the phenyl fragments did not undergo significant shifts and were in the region of 7.30–7.43 ppm for the ligand and 7.27–7.42 for complex **2a**. The  $^{13}\text{C}$  spectra also showed changes in the chemical shifts in complexes **2a,b** compared to the starting phenylalanine. Thus, the values of 55.81 and 57.42 for  $^2\text{C}$  and 36.18 and 40.59 for  $^3\text{C}$  were found for the ligand and complex **2a**, respectively (Supplementary Materials).

The powder diffraction patterns of composites **1,2** were recorded across  $2\theta = 5\text{--}60^\circ$ . The XRD patterns of composites **1,2** showed well-defined crystalline peaks defined by their crystalline nature (Figure 1). Thus, according to XRD data, the maxima of composite **1** were at 5.410 (100%) and 20.10 (73%) of  $[\text{Cu}(S\text{-Ala})_2]\text{--}[\text{Cu}(S\text{-Phe})_2]$  (**1**) (Figure 1a). For composite **2**, the maxima were at 20.28 (100%) and 22.10 (52%) (Figure 1b).

The IR spectra of **1,2** in the region of characteristic vibrations showed that the compounds obtained were mixed chelate complexes without an admixture of the starting amino acids (Figure 2).

In fact, comparison of the IR spectra of the starting amino acids (*S*-phenylalanine, *S*-alanine) and the resulting mixed chelate composites ( $[\text{Cu}(S\text{-Ala})_2]\text{--}[\text{Cu}(S\text{-Phe})_2]$  (**1**) and  $[\text{Zn}(S\text{-Ala})_2(\text{H}_2\text{O})]\text{--}[\text{Zn}(S\text{-Phe})_2(\text{H}_2\text{O})]$  (**2**)) showed that a shift of characteristic absorption bands occurred upon complexation. A shift was observed in the long-wavelength region for frequencies associated with symmetric and asymmetric absorption bands of the C–O bond of the carboxylate ion  $\nu_{\text{as,s}}(\text{C–O}) + \delta(\text{CH})$  and in the short-wavelength region for the stretching vibrations of the carbonyl group  $\nu_{\text{as,s}}(\text{C=O})$  relative to the absorption bands of the original amino acids (Figure 2). At the same time, an increase in the value of  $\Delta\nu(\text{COO})$  [38] indicated that chelate complexes were formed.

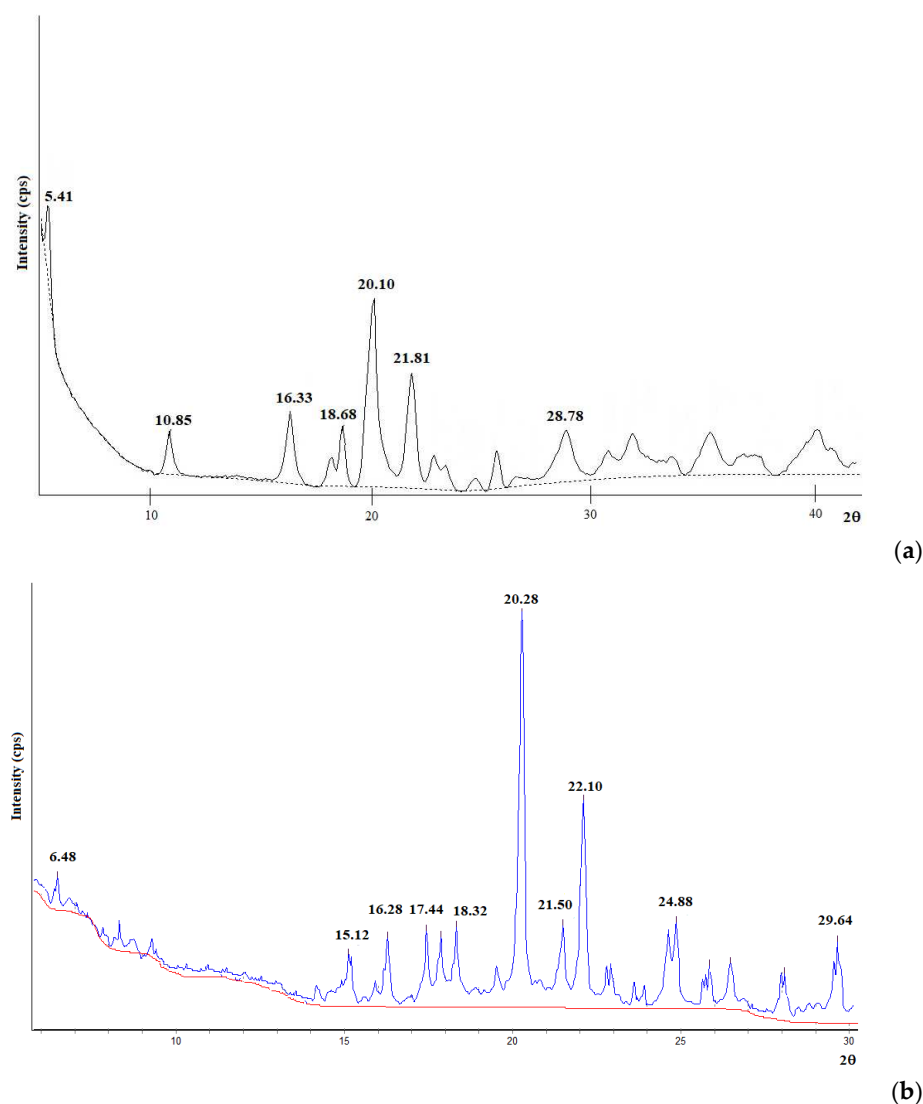


**Figure 1.** XRD pattern of composite  $[\text{Cu}(\text{S-Ala})_2]\text{-}[\text{Cu}(\text{S-Phe})_2]$  (**1**) (**a**) and composite  $[\text{Zn}(\text{S-Ala})_2(\text{H}_2\text{O})]\text{-}[\text{Zn}(\text{S-Phe})_2(\text{H}_2\text{O})]$  (**2**) (**b**).

In addition, the IR spectra of composites **1,2** contained no absorption bands responsible for the bending vibrations of the protonated amino group  $\delta(\text{NH}_3^+)$ , which is characteristic of the “zwitterion” of the original amino acids (Figure 2).

Additionally, a quantum-chemical simulation of the monomer link for complexes **1a,b** and **2a,b** was carried out using the M06/6-311+G(d) method [39]. The *ta-te* conformer of complexes **1a,b** and **2a,b** was chosen as a model for the study as the most energetically favorable one for the trans-isomer [31,32].

In this work we compared the enantioselectivity of voltammetric sensors using certain  $\alpha$ -amino acids (*S*-AlaH, *S*-PheH,  $[\text{Cu}(\text{S-Ala})_2]$ ,  $[\text{Cu}(\text{S-Phe})_2]$ ,  $[\text{Zn}(\text{S-Ala})_2(\text{H}_2\text{O})]$ ,  $[\text{Zn}(\text{S-Phe})_2(\text{H}_2\text{O})]$ ) or composites ( $[\text{Cu}(\text{S-Ala})_2]\text{-}[\text{Cu}(\text{S-Phe})_2]$  (**1**) and  $[\text{Zn}(\text{S-Ala})_2(\text{H}_2\text{O})]\text{-}[\text{Zn}(\text{S-Phe})_2(\text{H}_2\text{O})]$  (**2**)) as the chiral selectors. The schemes of electrooxidation of analytes are presented in Table 1. After recording the differential-pulse voltammograms (DPV) of *R*- and *S*-naproxen (Nap) (Figure 3) and *R*- and *S*-propranolol (Prp) (Figure 4) enantiomers, we compared the changes in the oxidation potentials of the enantiomers on the suggested sensors and the enantioselectivity coefficients ( $i_{pS}/i_{pR}$ ) (Table 2). The first oxidation peak was considered as the Nap analytical signal, since the  $i_{p1S}/i_{p1R}$  selectivity coefficient is larger than  $i_{p2S}/i_{p2R}$ .

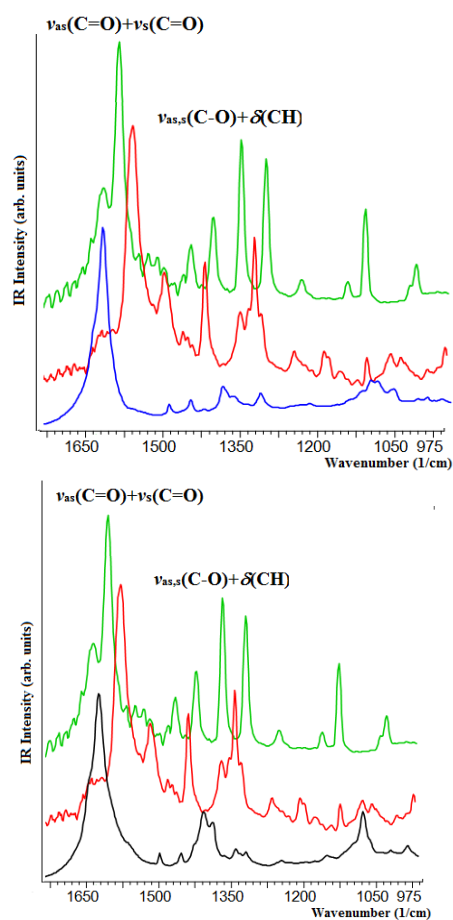


**Figure 2.** Fragments of IR spectra in the range of characteristic stretching vibrations of *S*-PheH (green), *S*-AlaH (red), **1** (blue), and **2** (black).

**Table 1.** Schemes of electrooxidation of the analytes.

| Analyte | Electrooxidation Scheme | Reference |
|---------|-------------------------|-----------|
| Nap     | <p>Ar = </p>            | [40]      |
| Prp     |                         | [41]      |

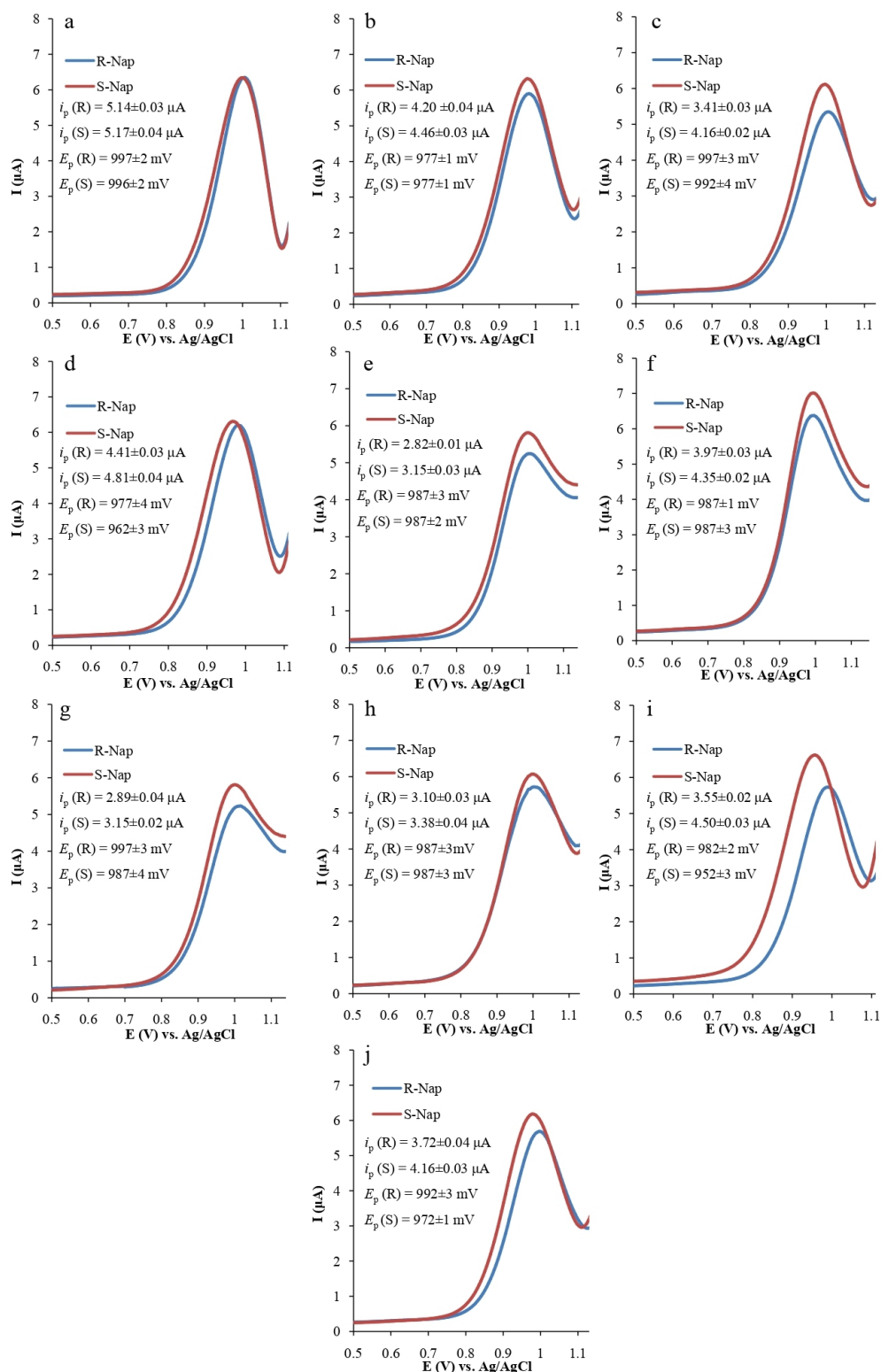


**Figure 3.** DPV of 1 mM solutions of R- and S-Nap on (a) GCE, (b) GCE/PEC, (c) GCE/PEC-(S-AlaH), (d) GCE/PEC-(S-PheH), (e) GCE/PEC-[Cu(S-PheH)<sub>2</sub>], (f) GCE/PEC-[Zn(S-PheH)<sub>2</sub>(H<sub>2</sub>O)], (g) GCE/PEC-[Cu(S-AlaH)<sub>2</sub>], (h) GCE/PEC-[Zn(S-AlaH)<sub>2</sub>(H<sub>2</sub>O)], (i) GCE/PEC-[Cu(S-Ala)<sub>2</sub>]-[Cu(S-Phe)<sub>2</sub>], and (j) GCE/PEC-[Zn(S-Ala)<sub>2</sub>(H<sub>2</sub>O)]-[Zn(S-Phe)<sub>2</sub>(H<sub>2</sub>O)] (phosphate buffer solution with pH 6.86, potential scanning rate 0.2 V/s).

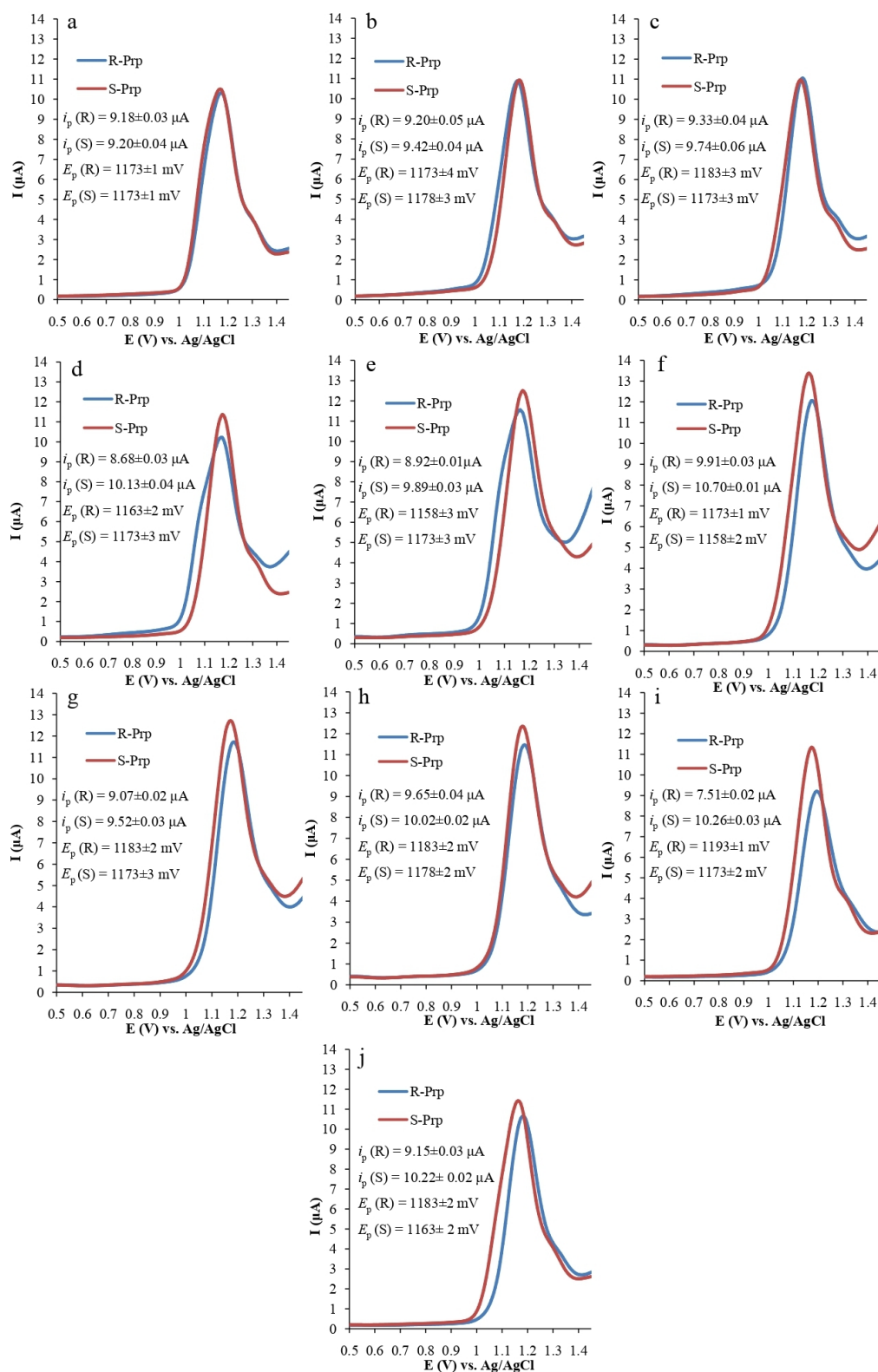


**Figure 4.** DPV of 1 mM solutions of R- and S-Prp on (a) GCE, (b) GCE/PEC, (c) GCE/PEC-(S-AlaH), (d) GCE/PEC-(S-PheH), (e) GCE/PEC-[Cu(S-PheH)<sub>2</sub>], (f) GCE/PEC-[Zn(S-PheH)<sub>2</sub>(H<sub>2</sub>O)], (g) GCE/PEC-[Cu(S-AlaH)<sub>2</sub>], (h) GCE/PEC-[Zn(S-AlaH)<sub>2</sub>(H<sub>2</sub>O)], (i) GCE/PEC-[Cu(S-Ala)<sub>2</sub>]-[Cu(S-Phe)<sub>2</sub>], and (j) GCE/PEC-[Zn(S-Ala)<sub>2</sub>(H<sub>2</sub>O)]-[Zn(S-Phe)<sub>2</sub>(H<sub>2</sub>O)] (0.05 M sulfuric acid, potential scanning rate 0.2 V/s).

**Table 2.** Comparison of the enantioselectivity of unmodified and modified sensors based on a GCE.

| Sensor  | Analyte * | $\Delta E_p$ , mV | $i_{pS}/i_{pR}$ |
|---|-----------|-------------------|-----------------|
| GCE   |           | 0                 | 1.00            |
| GCE/PEC   |           | 0                 | 1.06            |
| GCE/PEC-(S-AlaH)  |           | 5                 | 1.22            |
| GCE/PEC-(S-PheH)  |           | 15                | 1.09            |
| GCE/PEC-[Cu(S-PheH) <sub>2</sub> ]  | Nap       | 0                 | 1.12            |
| GCE/PEC-[Zn(S-Phe) <sub>2</sub> (H <sub>2</sub> O)]   |           | 0                 | 1.10            |
| GCE/PEC-[Cu(S-AlaH) <sub>2</sub> ]  |           | 10                | 1.09            |
| GCE/PEC-[Zn(S-AlaH) <sub>2</sub> (H <sub>2</sub> O)]  |           | 0                 | 1.09            |
| GCE/PEC GCE/PEC-[Cu(S-Ala) <sub>2</sub> ]-[Cu(S-Phe) <sub>2</sub> ]                             |           | 30                | 1.27            |
| GCE/PEC-[Zn(S-Ala) <sub>2</sub> (H <sub>2</sub> O)]-[Zn(S-Phe) <sub>2</sub> (H <sub>2</sub> O)] |           | 20                | 1.12            |
| GCE   |           | 0                 | 1.00            |
| GCE/PEC   |           | 5                 | 1.02            |
| GCE/PEC-(S-AlaH)  |           | 10                | 1.04            |
| GCE/PEC-(S-PheH)  |           | 10                | 1.17            |
| GCE/PEC-[Cu(S-PheH) <sub>2</sub> ]  | Prp       | 15                | 1.11            |
| GCE/PEC-[Zn(S-Phe) <sub>2</sub> (H <sub>2</sub> O)]   |           | 15                | 1.08            |
| GCE/PEC-[Cu(S-AlaH) <sub>2</sub> ]  |           | 10                | 1.05            |
| GCE/PEC-[Zn(S-AlaH) <sub>2</sub> (H <sub>2</sub> O)]  |           | 5                 | 1.04            |
| GCE/PEC-[Cu(S-Ala) <sub>2</sub> ]-[Cu(S-Phe) <sub>2</sub> ]                                     |           | 20                | 1.37            |
| GCE/PEC-[Zn(S-Ala) <sub>2</sub> (H <sub>2</sub> O)]-[Zn(S-Phe) <sub>2</sub> (H <sub>2</sub> O)] |           | 20                | 1.12            |

\* 1mM solutions of enantiomers; phosphate buffer solution with pH 6.86 for Nap and 0.5 M sulfuric acid for Prp; potential scanning rate 0.2 V/s.

If only a polyelectrolyte complex (PEC), which is used as a substrate for fixing the chiral selector, was applied onto glassy carbon electrode (GCE), insignificant differences in the analytical signals of the Nap and Prp enantiomers were observed (Table 2), which indicated that due to its functional groups, this complex exhibited small enantioselectivity with respect to the enantiomers. The addition of amino acids S-AlaH or S-PheH (Figures 3c,d and 4c,d) or individual complexes [M(S-Ala)<sub>2</sub>(H<sub>2</sub>O)<sub>n</sub>], [M(S-Phe)<sub>2</sub>(H<sub>2</sub>O)<sub>n</sub>] (M = Cu(II), Zn(II); n = 0–1) (Figures 3e,f and 4e,f) to the PEC slightly increased the enantioselectivity of the sensor (Table 2). In this case, enantioselectivity reached 15 mV for  $\Delta E_p$  and 1.22 for  $i_{pS}/i_{pR}$ , while the enantioselectivity growth by  $i_{pS}/i_{pR}$  did not exceed 15%.

A significant improvement of the sensor enantioselectivity could be obtained by using a mixture of the complexes studied as the chiral modifiers (Table 2). The best result was demonstrated by the GCE/PEC-[Cu(S-Ala)<sub>2</sub>]-[Cu(S-Phe)<sub>2</sub>] sensor that used a mixture of [Cu(S-Ala)<sub>2</sub>] and [Cu(S-Phe)<sub>2</sub>] (1) in a 1:1 ratio. This sensor demonstrated an enantioselectivity coefficient of  $i_{pS}/i_{pR} = 1.27$  and  $\Delta E_p = 30$  mV for Nap;  $i_{pS}/i_{pR} = 1.37$  and  $\Delta E_p = 20$  mV for Prp. We note that a mixture of complexes provided an unexpectedly high increase in the sensor enantioselectivity. The enantioselectivity coefficient  $i_{pS}/i_{pR}$  increased up to 29% instead of the expected 15%. The increase in  $\Delta E_p$  up to 30 mV was also much larger than the value of 15 mV that was obtained for chiral modifiers based on individual compounds. Obviously, in the case of a mixture of complexes, a synergetic effect may be suggested. The nature of this effect is not clear yet, but we believe that an important role is played by the presence of a compound with an alternate structure of ligands at the optical center. As a result, interaction of a chiral analyte, Nap or Prp, with a mixed-type chiral selector (M<sub>1</sub> + M<sub>2</sub>) on the sensor surface assumes the formation of, at least, mixed-type associates, e.g., S-Nap \* (M<sub>1</sub>, M<sub>2</sub>)<sub>n</sub>, instead of unmixed-type associates S-Nap \* (M)<sub>n</sub> for an individual chiral selector. Such mixed-type associates contain more differing optically active centers; therefore, the difference in the properties, including  $\Delta E_p$  and  $i$ , between S-Nap \* (M<sub>1</sub>, M<sub>2</sub>)<sub>n</sub> and R-Nap \* (M<sub>1</sub>, M<sub>2</sub>)<sub>n</sub> is more pronounced.

To estimate the sensitivity of the suggested sensors, measurements were performed in solutions of Nap and Prp enantiomers with known concentrations. The DPV of Nap and Prp enantiomers are shown in Figure 5, Figure 6, Figures 7 and 8, respectively, along with the calibration plot (insets in Figures 5–8). Linear relationships between the anodic current

and the concentration of analyte enantiomers were obtained in the range of  $2.5 \times 10^{-5}$  to  $1.0 \times 10^{-3}$  mol L<sup>-1</sup> on the GCE/PEC-[Cu(S-Ala)<sub>2</sub>]-[Cu(S-Phe)<sub>2</sub>] sensor and  $5.0 \times 10^{-5}$  to  $1.0 \times 10^{-3}$  on the GCE/PEC-[Zn(S-Ala)<sub>2</sub>(H<sub>2</sub>O)]-[Zn(S-Phe)<sub>2</sub>(H<sub>2</sub>O)] sensor (five measurements for each enantiomer). The limit of detection (LOD) (3 s/m) and the limit of quantification (LOQ) (10 s/m), where s is the standard deviation and m is the slope of the calibration curves, were found to be 0.30 μM and 0.99 μM for S-Nap, 0.38 μM and 1.25 μM for R-Nap, 0.90 μM and 3.02 μM for S-Prp, and 1.24 μM and 4.15 μM for R-Prp μM, respectively, on GCE/PEC-[Cu(S-Ala)<sub>2</sub>]-[Cu(S-Phe)<sub>2</sub>]; 0.38 μM and 1.26 μM for S-Nap, 0.42 μM and 1.40 μM for R-Nap, 0.78 μM and 2.62 μM for S-Prp, and 0.87 μM and 2.91 μM for R-Prp μM, respectively, on GCE/PEC-[Zn(S-Ala)<sub>2</sub>(H<sub>2</sub>O)]-[Zn(S-Phe)<sub>2</sub>(H<sub>2</sub>O)]. These results confirmed that the suggested composite sensors can be used in the chiral detection of Nap and Prp enantiomers.

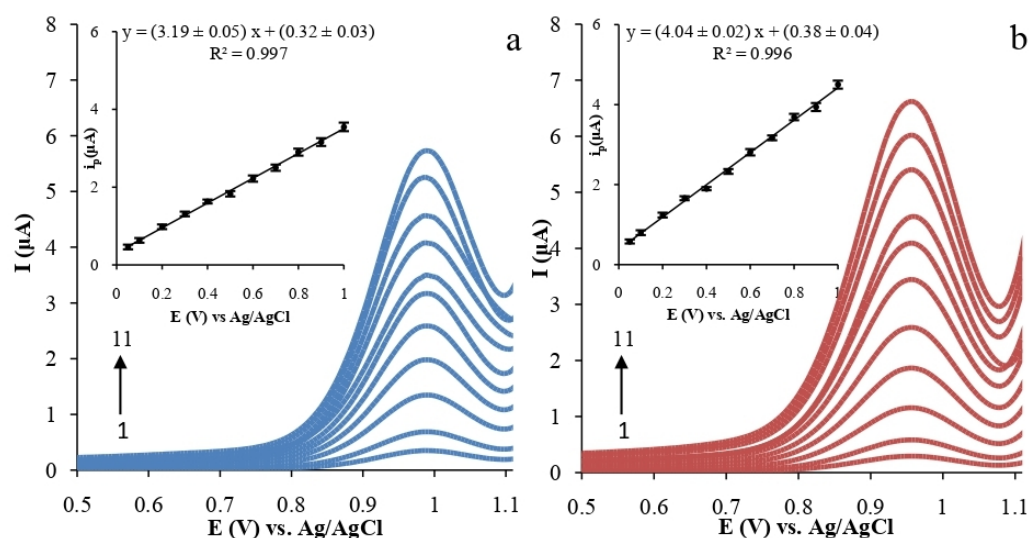


**Figure 5.** DPV of (a) R-Nap and (b) S-Nap solutions of various concentrations on GCE/PEC-[Cu(S-Ala)<sub>2</sub>]-[Cu(S-Phe)<sub>2</sub>]: 0.05 (1), 0.1 (2), 0.2 (3), 0.3 (4), 0.4 (5), 0.5 (6), 0.6 (7), 0.7 (8), 0.8 (9), 0.9 (10), 1 (11) mM (phosphate buffer solution with pH 6.86, potential scanning rate 0.2 V/s). Insets: the corresponding calibration curves.

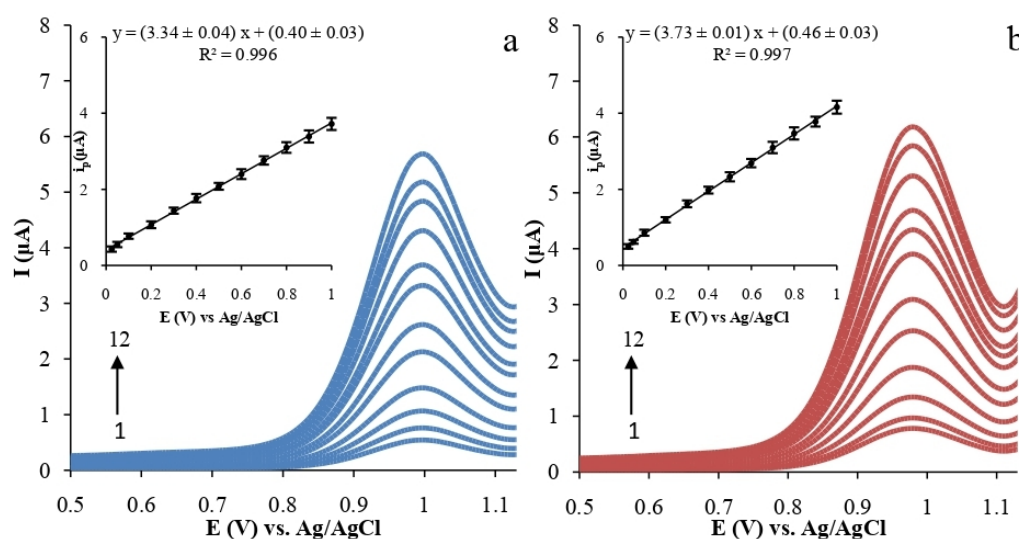


**Figure 6.** DPV of (a) R-Nap and (b) S-Nap solutions of various concentrations on GCE/PEC-[Zn(S-Ala)<sub>2</sub>(H<sub>2</sub>O)]-[Zn(S-Phe)<sub>2</sub>(H<sub>2</sub>O)]: 0.025 (1), 0.05 (2), 0.1 (3), 0.2 (4), 0.3 (5), 0.4 (6), 0.5 (7), 0.6 (8), 0.7 (9), 0.8 (10), 0.9 (11), 1 (12) mM (phosphate buffer solution with pH 6.86, potential scanning rate 0.2 V/s). Insets: the corresponding calibration curves.

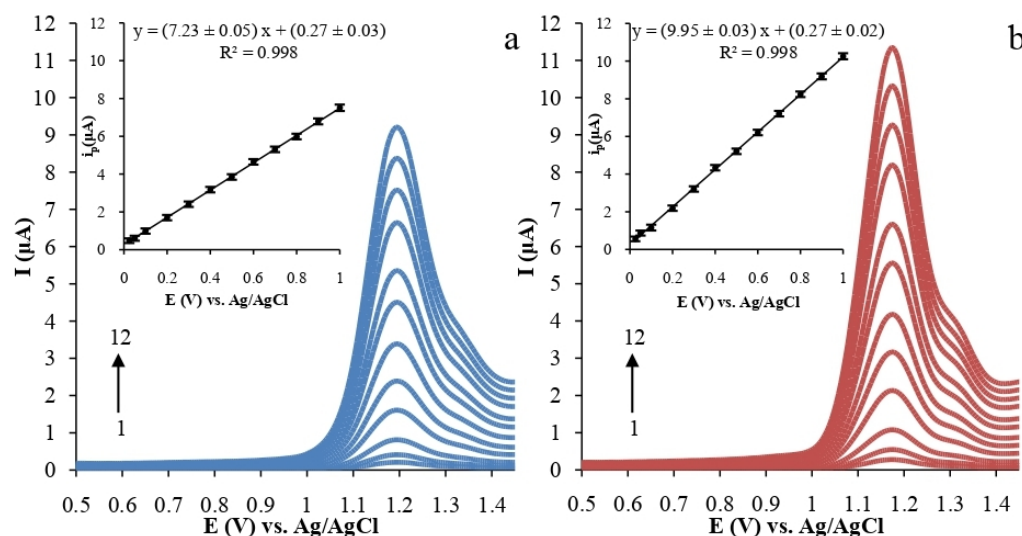


**Figure 7.** DPV of (a) R-Prp and (b) S-Prp solutions of various concentrations on GCE/PEC-[Cu(S-Ala)<sub>2</sub>]-[Cu(S-Phe)<sub>2</sub>]: 0.025 (1), 0.05 (2), 0.1 (3), 0.2 (4), 0.3 (5), 0.4 (6), 0.5 (7), 0.6 (8), 0.7 (9), 0.8 (10), 0.9 (11), 1 (12) mM (0.05 M sulfuric acid, potential scanning rate 0.2 V/s). Insets: the corresponding calibration curves.

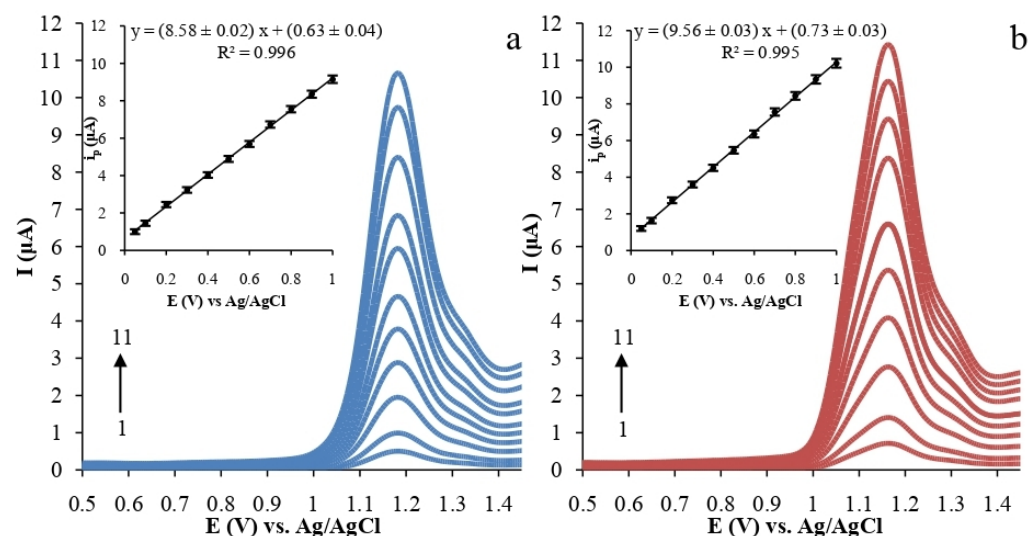


**Figure 8.** DPV of (a) R-Prp and (b) S-Prp solutions of various concentrations on GCE/PEC-[Zn(S-Ala)<sub>2</sub>(H<sub>2</sub>O)]-[Zn(S-Phe)<sub>2</sub>(H<sub>2</sub>O)]: 0.05 (1), 0.1 (2), 0.2 (3), 0.3 (4), 0.4 (5), 0.5 (6), 0.6 (7), 0.7 (8), 0.8 (9), 0.9 (10), 1 (11) mM (0.05 M sulfuric acid, potential scanning rate 0.2 V/s). Insets: the corresponding calibration curves.

Table 3 compares the sensors we developed with other reported electrochemical chiral sensors developed for the enantio-differentiation of Nap and Prp. The suggested sensors enable the discrimination of Nap and Prp enantiomers with a wider linear range compared to many sensors reported in literature. The values of LOD obtained with the present sensors were comparable, or in some cases lower than those obtained with other fabricated electrochemical sensors [41–52].

**Table 3.** Comparison of various modified electrodes for recognition of Prp and Nap enantiomers.

| Sensor  | Electro-Chemical Technique | Linear Range, Mol L <sup>-1</sup>               | LOD, μmol L <sup>-1</sup>        | Reference |
|---|----------------------------|---|----------------------------------|-----------|
| Nap enantiomers   |                            |   |                                  |           |
| GCE/PEC-[Cu(S-Ala) <sub>2</sub> ]-[Cu(S-Phe) <sub>2</sub> ]                                     | DPV                        | 2.5 × 10 <sup>-5</sup> -1.0 × 10 <sup>-3</sup>  | 0.30 for S-Nap<br>0.38 for R-Nap | this work |
| GCE/PEC-[Zn(S-Ala) <sub>2</sub> (H <sub>2</sub> O)]-[Zn(S-Phe) <sub>2</sub> (H <sub>2</sub> O)] | DPV                        | 5.0 × 10 <sup>-5</sup> -1.0 × 10 <sup>-3</sup>  | 0.38 for S-Nap<br>0.42 for R-Nap | this work |
| Au@BSA  | DPV                        | 1.0 × 10 <sup>-5</sup> -5.0 × 10 <sup>-3</sup>  | 3.3                              | [41]      |
| β-CD/EG/GCEMB@β-CD/EG/GCE   | DPV                        | 4.0 × 10 <sup>-7</sup> -6.0 × 10 <sup>-6</sup>  | 0.07                             | [42]      |
| L-Cys/RGO/GCE   | CV                         | 5.0 × 10 <sup>-6</sup> -1.3 × 10 <sup>-4</sup>  | 0.35 for S-Nap<br>2.5 for R-Nap  | [43]      |
| L-CYS/AuNPs/Au  | CV                         | 2.0 × 10 <sup>-6</sup> -2.0 × 10 <sup>-5</sup>  | 0.67                             | [44]      |
| BSA/TBO@rGO/GCE   | CV                         | 5.0 × 10 <sup>-4</sup> -5.0 × 10 <sup>-3</sup>  | 0.33                             | [45]      |
| Prp enantiomers   |                            |   |                                  |           |
| GCE/PEC-[Cu(S-Ala) <sub>2</sub> ]-[Cu(S-Phe) <sub>2</sub> ]                                     | DPV                        | 2.5 × 10 <sup>-5</sup> -1.0 × 10 <sup>-3</sup>  | 0.90 for S-Prp<br>1.24 for R-Prp | this work |
| GCE/PEC-[Zn(S-Ala) <sub>2</sub> (H <sub>2</sub> O)]-[Zn(S-Phe) <sub>2</sub> (H <sub>2</sub> O)] | DPV                        | 5.0 × 10 <sup>-5</sup> -1.0 × 10 <sup>-3</sup>  | 0.78 for S-Prp<br>0.87 for R-Prp | this work |
| CNT-silicone-rubber-CPE   | DPV                        | 5.0 × 10 <sup>-7</sup> -7.0 × 10 <sup>-6</sup>  | 0.12                             | [46]      |
| PDMS-CPE  | DPV                        | 1.0 × 10 <sup>-5</sup> -6.0 × 10 <sup>-5</sup>  | 3                                | [47]      |
| GCE/PAP/α-CD GCE/PAP/β-CD<br>GCE/PAP/MAGCE/PAP/CA   | DPV                        | 2.1 × 10 <sup>-5</sup> -6.75 × 10 <sup>-4</sup> | 5.46 ÷ 8.37                      | [48]      |
| MIP/rGO/GCE   | DPV                        | 5.0 × 10 <sup>-5</sup> -1.0 × 10 <sup>-3</sup>  | -                                | [49]      |
| CuNPs- GO-CB-PEDOT:PSS/GCE  | SWV                        | 5.0 × 10 <sup>-7</sup> -2.9 × 10 <sup>-6</sup>  | 0.18                             | [50]      |
| AgNP-IL-FG/GCE  | SWV                        | 1.0 × 10 <sup>-7</sup> -2.9 × 10 <sup>-6</sup>  | 0.017                            | [51]      |
| ctDNA/nanoAu-MB-MWNTs/GCE   | CV                         | 1.0 × 10 <sup>-5</sup> -5.0 × 10 <sup>-3</sup>  | 3.3                              | [52]      |

The validity of results of determination of Nap and Prp enantiomers by the suggested composite sensors was estimated by the “added–found” method (Table 4). It was found that the sensors made it possible to determine the content of Nap and Prp enantiomers with high accuracy in a wide concentration range. The relative standard deviation did not exceed 2.2% in the determination of Nap enantiomers and 1.9% for Prp enantiomers in model solutions. The developed enantioselective sensors were used to determine Nap and Prp enantiomers in biological fluids. Statistical assessment of results of determination by the “added–found” method indicated the absence of systematic error. The relative standard deviation in the determination of enantiomers in biological fluids ranged within 1.9–4.7%. Thus, the suggested sensors are suitable for highly reproducible determination of Nap and Prp enantiomers in biological fluids.

**Table 4.** DPV determination of R- and S-Nap (phosphate buffer solution with pH 6.86) and R- and S-Prp (0.05 M sulfuric acid) in model solutions on GCE modified by PEC composites [M(S-Ala)<sub>2</sub>(H<sub>2</sub>O)<sub>n</sub>]-[M(S-Phe)<sub>2</sub>(H<sub>2</sub>O)<sub>n</sub>] (M = Cu(II), Zn(II); n = 0–1) (potential scanning rate 0.2 Vs<sup>-1</sup>, n = 5, p = 0.95).

| Sensor  | Added, μM |     | Found, μM |         | Recovery, % |       | RSD, % |     |
|---|-----------|-----|-----------|---------|-------------|-------|--------|-----|
|   | R         | S   | R         | S       | R           | S     | R      | S   |
| Solutions of Nap enantiomers  |           |     |           |         |             |       |        |     |
| GCE/PEC-[Cu(S-Ala) <sub>2</sub> ]-[Cu(S-Phe) <sub>2</sub> ]                                     | 75        | 75  | 74 ± 2    | 75 ± 2  | 98.7        | 100.0 | 1.8    | 2.1 |
|   | 250       | 250 | 249 ± 7   | 249 ± 6 | 99.6        | 99.6  | 2.2    | 2.1 |
|   | 750       | 750 | 747 ± 9   | 752 ± 8 | 99.6        | 100.3 | 1.0    | 0.9 |
|   | 75        | 75  | 74 ± 2    | 75 ± 3  | 98.7        | 100.0 | 1.9    | 1.8 |
| GCE/PEC-[Zn(S-Ala) <sub>2</sub> (H <sub>2</sub> O)]-[Zn(S-Phe) <sub>2</sub> (H <sub>2</sub> O)] | 250       | 250 | 249 ± 3   | 251 ± 3 | 99.6        | 100.4 | 1.9    | 1.6 |
|   | 750       | 750 | 751 ± 6   | 751 ± 5 | 100.1       | 100.1 | 1.1    | 0.9 |

Table 4. Cont.

| Sensor  | Added, $\mu\text{M}$ |     | Found, $\mu\text{M}$ |         | Recovery, % |       | RSD, % |     |
|---|----------------------|-----|----------------------|---------|-------------|-------|--------|-----|
|   | R                    | S   | R                    | S       | R           | S     | R      | S   |
| Nap enantiomers in human blood plasma   |                      |     |                      |         |             |       |        |     |
| GCE/PEC-[Cu(S-Ala) <sub>2</sub> ]-[Cu(S-Phe) <sub>2</sub> ]                                     | 75                   | 75  | 72 ± 3               | 73 ± 3  | 96.0        | 97.3  | 3.8    | 2.9 |
|   | 250                  | 250 | 245 ± 9              | 245 ± 8 | 98.0        | 98.0  | 3.0    | 2.6 |
|   | 750                  | 750 | 745 ± 9              | 749 ± 7 | 99.3        | 99.9  | 2.9    | 2.4 |
| GCE/PEC-[Zn(S-Ala) <sub>2</sub> (H <sub>2</sub> O)]-[Zn(S-Phe) <sub>2</sub> (H <sub>2</sub> O)] | 75                   | 75  | 72 ± 4               | 72 ± 4  | 96.0        | 96.0  | 4.7    | 4.5 |
|   | 250                  | 250 | 245 ± 5              | 248 ± 7 | 98.0        | 99.2  | 2.6    | 2.2 |
|   | 750                  | 750 | 747 ± 8              | 747 ± 5 | 99.6        | 99.6  | 2.9    | 2.5 |
| Nap enantiomers in urine  |                      |     |                      |         |             |       |        |     |
| GCE/PEC-[Cu(S-Ala) <sub>2</sub> ]-[Cu(S-Phe) <sub>2</sub> ]                                     | 75                   | 75  | 73 ± 5               | 74 ± 4  | 97.3        | 98.7  | 3.8    | 3.6 |
|   | 250                  | 250 | 246 ± 8              | 248 ± 7 | 98.4        | 99.2  | 2.9    | 2.5 |
|   | 750                  | 750 | 746 ± 4              | 751 ± 9 | 99.5        | 100.1 | 2.7    | 2.3 |
| GCE/PEC-[Zn(S-Ala) <sub>2</sub> (H <sub>2</sub> O)]-[Zn(S-Phe) <sub>2</sub> (H <sub>2</sub> O)] | 75                   | 75  | 72 ± 3               | 73 ± 3  | 96.0        | 97.3  | 3.0    | 3.1 |
|   | 250                  | 250 | 247 ± 4              | 249 ± 8 | 98.8        | 99.6  | 2.7    | 2.3 |
|   | 750                  | 750 | 749 ± 6              | 749 ± 4 | 99.9        | 99.9  | 2.4    | 2.0 |
| Solutions of Prp enantiomers  |                      |     |                      |         |             |       |        |     |
| GCE/PEC-[Cu(S-Ala) <sub>2</sub> ]-[Cu(S-Phe) <sub>2</sub> ]                                     | 75                   | 75  | 74 ± 2               | 75 ± 2  | 98.7        | 100.0 | 1.9    | 1.8 |
|   | 250                  | 250 | 248 ± 5              | 251 ± 4 | 99.2        | 99.2  | 1.6    | 1.3 |
|   | 750                  | 750 | 747 ± 5              | 752 ± 4 | 99.6        | 100.3 | 0.9    | 0.7 |
| GCE/PEC-[Zn(S-Ala) <sub>2</sub> (H <sub>2</sub> O)]-[Zn(S-Phe) <sub>2</sub> (H <sub>2</sub> O)] | 75                   | 75  | 74 ± 2               | 76 ± 2  | 98.7        | 101.3 | 1.8    | 1.7 |
|   | 250                  | 250 | 248 ± 3              | 248 ± 4 | 99.2        | 99.2  | 0.9    | 1.2 |
|   | 750                  | 750 | 745 ± 7              | 751 ± 5 | 99.3        | 100.1 | 0.7    | 0.5 |
| Prp enantiomers in human blood plasma   |                      |     |                      |         |             |       |        |     |
| GCE/PEC-[Cu(S-Ala) <sub>2</sub> ]-[Cu(S-Phe) <sub>2</sub> ]                                     | 75                   | 75  | 72 ± 4               | 73 ± 2  | 96.0        | 97.3  | 3.6    | 2.2 |
|   | 250                  | 250 | 245 ± 9              | 245 ± 8 | 98.0        | 98.0  | 3.0    | 2.7 |
|   | 750                  | 750 | 745 ± 9              | 748 ± 7 | 99.3        | 99.7  | 2.5    | 2.4 |
| GCE/PEC-[Zn(S-Ala) <sub>2</sub> (H <sub>2</sub> O)]-[Zn(S-Phe) <sub>2</sub> (H <sub>2</sub> O)] | 75                   | 75  | 72 ± 4               | 73 ± 4  | 96.0        | 97.3  | 3.7    | 3.5 |
|   | 250                  | 250 | 247 ± 7              | 247 ± 7 | 98.8        | 98.8  | 2.1    | 2.3 |
|   | 750                  | 750 | 746 ± 6              | 748 ± 4 | 99.5        | 99.7  | 2.0    | 2.1 |
| Prp enantiomers in urine  |                      |     |                      |         |             |       |        |     |
| GCE/PEC-[Cu(S-Ala) <sub>2</sub> ]-[Cu(S-Phe) <sub>2</sub> ]                                     | 75                   | 75  | 73 ± 2               | 74 ± 2  | 97.3        | 98.7  | 2.3    | 2.2 |
|   | 250                  | 250 | 246 ± 8              | 247 ± 4 | 98.4        | 98.8  | 2.6    | 2.4 |
|   | 750                  | 750 | 746 ± 5              | 752 ± 7 | 99.5        | 100.3 | 2.1    | 2.0 |
| GCE/PEC-[Zn(S-Ala) <sub>2</sub> (H <sub>2</sub> O)]-[Zn(S-Phe) <sub>2</sub> (H <sub>2</sub> O)] | 75                   | 75  | 73 ± 3               | 74 ± 1  | 97.3        | 98.7  | 3.0    | 2.5 |
|   | 250                  | 250 | 248 ± 5              | 249 ± 2 | 99.2        | 99.6  | 2.2    | 2.0 |
|   | 750                  | 750 | 749 ± 8              | 749 ± 5 | 99.9        | 99.9  | 2.0    | 1.9 |

### 3. Materials and Methods

All the reagents and chemicals were purchased from commercial sources (PanReac AppliChem; Sigma Aldrich) and were used as received without further purification. All the solutions were prepared by standard methods. XRD analysis was performed with a Bruker D8 Advance X-ray diffractometer. Cu K $\alpha$  radiation with Bragg–Brentano focusing was used. Solid samples of complexes **1** and **2** (about 30 mg of the powder) were ground with a pestle in a porcelain mortar. FTIR spectra were recorded on an FTIR-8400 S spectrometer (Shimadzu, Tokyo, Japan) (4000–400 cm<sup>-1</sup>, 2 cm<sup>-1</sup> resolution, 20 scans) at 25 °C. <sup>1</sup>H and <sup>13</sup>C NMR spectra were recorded on a Bruker Avance-III 500 MHz spectrometer (500.13 MHz (<sup>1</sup>H), 125.75 MHz (<sup>13</sup>C)). The samples were prepared in standard tubes 5 mm in diameter. One and two-dimensional NMR spectra (<sup>1</sup>H, <sup>1</sup>H) COSY, (<sup>1</sup>H, <sup>13</sup>C) HSQC, (<sup>1</sup>H, <sup>13</sup>C) HMBC were measured using standard pulse sequences. The ESI-MS spectrum was recorded on an LCMS-2010EV HPLC mass-spectrometer (Shimadzu, Tokyo, Japan).

The quantum chemical simulation of the complexes [Cu(S-Ala)<sub>2</sub>], [Cu(S-Phe)<sub>2</sub>] (**1a,b**) and [Zn(S-Ala)<sub>2</sub>(H<sub>2</sub>O)], [Zn(S-Phe)<sub>2</sub>(H<sub>2</sub>O)] (**2a,b**) was performed using density functional theory. The M06 functionals [39] were used in combination with the triple-valence split polarization basis set augmented with the set of sp-diffuse functions 6–311+G(d) [53–57]. The quantum chemical calculations were performed on a cluster supercomputer of the Ufa

Institute of Chemistry of the RAS using Gaussian 09 [58]. Visualization was performed using the ChemCraft program [59].

Voltammetric measurements were carried out on an Autolab PGSTAT 204 potentiostat-galvanostat (MetrohmAutolab Ins., Utrecht, The Netherlands) with NOVA software in a standard three-electrode cell with a working GCE 3 mm in diameter, an auxiliary electrode made of a platinum plate, and a silver chloride reference electrode. Differential pulse voltammograms were recorded in the potential range from 0 to 1.6 in the case of Prp or from 0 to 1.8 V in the case of Nap using an amplitude of 25 mV, a time interval of 0.5 s, a modulation time of 0.05 s, and a potential scan rate of 20 mV/s. An electrochemical cell thermally controlled at  $25 \pm 0.1$  °C was filled with 20 mL of an analyte, and the current-voltage curves were recorded. The data set for each sample consisted of five parallel measurements, which was sufficient to obtain reproducible results. Before recording the voltammograms, the indicator electrode was kept for 5 s in the test solution.

R- and S-Prp ( $\geq 99\%$ ) (Sigma Aldrich) and R- and S-Nap ( $\geq 98\%$ ) (Sigma Aldrich) were used as the analytes. Solutions of Nap enantiomers (1 mM) were prepared by dissolving a sample of the substance in 100 mL of a phosphate buffer solution ( $\text{Na}_2\text{HPO}_4$  and  $\text{KH}_2\text{PO}_4$ ) with pH 6.86. Solutions of Prp enantiomers (1 mM) were prepared by dissolving a sample of the compound in 100 mL of sulfuric acid (0.05 M).

The  $[\text{Cu}(\text{S-Ala})_2]$ ,  $[\text{Cu}(\text{S-Phe})_2]$ ,  $[\text{Zn}(\text{S-Ala})_2(\text{H}_2\text{O})]$ ,  $[\text{Zn}(\text{S-Phe})_2(\text{H}_2\text{O})]$ ,  $[\text{Cu}(\text{S-Ala})_2]$ - $[\text{Cu}(\text{S-Phe})_2]$  (**1**), and  $[\text{Zn}(\text{S-Ala})_2(\text{H}_2\text{O})]$ - $[\text{Zn}(\text{S-Phe})_2(\text{H}_2\text{O})]$  (**2**) composites, and S-alanine (S-AlaH) or S-phenylalanine (S-PheH in “zwitterionic” form) with the PEC were used to modify the GCE.

Samples of chitosan and 99% sodium salt of N-succinylchitosan were purchased from CJSC Bioprogress. The procedure for obtaining the PEC based on chitosan hydrochloride (with a molecular weight of 30 kDa and a deacetylation degree of 75%) and the sodium salt of N-succinylchitosan (with a molecular weight of 200 kDa obtained from chitosan with a deacetylation degree of 82%) is described elsewhere [17]. To obtain a composite, a weighed portion (0.002 g) of the complex or an amino acid was dissolved in 2 mL of the PEC and kept for 6 min in an ultrasonic bath, followed by filtration on a white ribbon filter. The GCE was modified by placing 10  $\mu\text{L}$  of a solution of the chitosan PEC with a chiral selector introduced into it onto a carefully polished GCE surface, followed by evaporation of the solvent under an IR lamp at a temperature of 80 °C.

Complexes **1a** and **1b** were obtained according to the published methods [31,32]. In a 100 mL flask equipped with a magnetic stirrer, a solution of 0.2 g S-PheH or 0.107 g S-AlaH (1.2 mmol) in distilled water (7 mL) was prepared. An 1 M solution of NaOH (1.2 mmol) was added to an aqueous solution of S-pheH or S-AlaH, and the mixture was stirred for 30 min. Then an aqueous solution of  $\text{CuCl}_2$  (0.1 g, 0.6 mmol  $\text{CuCl}_2 \cdot 2\text{H}_2\text{O}$  in 5 mL) was added to the deprotonated form of the amino acid. The reaction mixture was stirred at room temperature for 3 h to give a violet powder. The complex **1a** [32] or **1b** obtained in this way was analyzed by FTIR spectroscopy (br. broad; vs. very strong; s. strong; m. medium; w. weak).

FTIR (KBr,  $\text{cm}^{-1}$ )  $[\text{Cu}(\text{S-Ala})_2]$  (**1b**): 3273–2939 m. ( $\nu_{\text{as,s}}(-\text{NH}_2) + \nu_{\text{as,s}}(\text{CH}, \text{CH}_2)$ ); 1628 vs. ( $\nu_{\text{as,s}}(\text{C}=\text{O})$ ); 1396 s., 1373 m. ( $\nu_{\text{as,s}}(\text{C}-\text{O}) + \delta(\text{CH})$ ); 1159 m., 1119 m., 1105 m., 1063 m. ( $\nu(\text{C}-\text{N}) + \delta(\text{NH}_2) + \delta(\text{CH})$ ).

Complexes **2a** and **2b** were obtained using the published methods [17,27]. In a 100 mL flask equipped with a magnetic stirrer, a solution of 0.2 g L-PheH or 0.107 g L-AlaH (1.2 mmol) in distilled water (7 mL) was prepared. A solution of  $\text{Zn}(\text{CH}_3\text{COO})_2$  (0.111 g, 0.6 mmol  $\text{Zn}(\text{CH}_3\text{COO})_2 \cdot 2\text{H}_2\text{O}$  in 5 mL) was added to a solution of amino acid L-pheH or L-AlaH. The reaction mixture was stirred at 30–35 °C for 24 h to give a white powder. The complex **2a** [32] or **2b** obtained in this way was analyzed by FTIR spectroscopy (br. broad; vs. very strong; s. strong; m. medium; w. weak).

FTIR (KBr,  $\text{cm}^{-1}$ )  $[\text{Zn}(\text{S-Ala})_2(\text{H}_2\text{O})]$  (**2b**): 3406–2837 m. ( $\nu_{\text{as,s}}(-\text{NH}_2) + \nu_{\text{as,s}}(\text{CH}, \text{CH}_2)$ ); 1601 vs. ( $\nu_{\text{as,s}}(\text{C}=\text{O})$ ); 1425 m, 1396 s., 1364 m. ( $\nu_{\text{as,s}}(\text{C}-\text{O}) + \delta(\text{CH})$ ); 1144 m., 1119 m., 1053 m. ( $\nu(\text{C}-\text{N}) + \delta(\text{NH}_2) + \delta(\text{CH})$ ).

Composites **1** and **2** were obtained by mixing the components in a ratio of 1:1:1. *S*-PheH 0.15 g (0.9 mmol) and *S*-AlaH 0.08 g (0.9 mmol) were dissolved in distilled water (10 mL) in a flask ( $V = 50$  mL) on a magnetic stirrer and stirred for 30 min. A solution (5 mL) containing 0.181 g (0.9 mmol)  $\text{Cu}(\text{CH}_3\text{COO})_2 \cdot \text{H}_2\text{O}$  or 0.166 g (0.9 mmol)  $\text{Zn}(\text{CH}_3\text{COO})_2 \cdot 2 \text{H}_2\text{O}$  was added to the resulting mixture that was then stirred for 24 h at room temperature until a suspension formed. The reaction solution of complex **2** was additionally heated to 30–35 °C. After the formation of a precipitate, the resulting complexes were washed twice with water on a filter and dried at room temperature in a desiccator over  $\text{CaCl}_2$ .

Light-violet fine crystalline powders of composite **1** were obtained in 48% yield, and white powders of complex **2** were obtained in 51% yield.

FTIR (KBr,  $\text{cm}^{-1}$ ) [ $\text{Cu}(\text{S-Ala})_2$ ]-[ $\text{Cu}(\text{S-Phe})_2$ ] (**1**): 3086–2928 m. ( $\nu_{\text{as,s}}(\text{-NH}_2) + \nu_{\text{as,s}}(\text{CH}, \text{CH}_2)$ ); 1620 vs. ( $\nu_{\text{as,s}}(\text{C=O})$ ); 1396 s., 1381 m. ( $\nu_{\text{as,s}}(\text{C-O}) + \delta(\text{CH})$ ); 1136 m., 1121 m., 1107 m., 1076 m. ( $\nu(\text{C-N}) + \delta(\text{NH}_2) + \delta(\text{CH})$ ).

FTIR (KBr,  $\text{cm}^{-1}$ ) [ $\text{Zn}(\text{S-Ala})_2(\text{H}_2\text{O})$ ]-[ $\text{Zn}(\text{S-Phe})_2(\text{H}_2\text{O})$ ] (**2**): 3475 m., 3414 m. ( $\nu(\text{OH})$ ); 3258–2854 m. ( $\nu_{\text{as,s}}(\text{-NH}_2) + \nu_{\text{as,s}}(\text{CH}, \text{CH}_2)$ ); 1620 vs. ( $\nu_{\text{as,s}}(\text{C=O})$ ); 1410 s., 1391 m. ( $\nu_{\text{as,s}}(\text{C-O}) + \delta(\text{CH})$ ); 1088 m. ( $\nu(\text{C-N}) + \delta(\text{NH}_2) + \delta(\text{CH})$ ). [ $\text{Zn}(\text{S-Phe})_2(\text{H}_2\text{O})$ ] (**2a**):  $^1\text{H}$  NMR ( $\text{D}_2\text{O}$ , 298 K),  $\delta$ , ppm: 7.31–7.42 (m, 5H, Ph), 3.79 (dd, 1H,  $\text{CH}_2\text{CH}$ ,  $^3\text{J} = 7.7$  Hz), 3.23 (dd, 1H,  $\text{CHH}$ ,  $^2\text{J} = 14.4$  Hz,  $^3\text{J} = 4.8$  Hz), 3.02 (dd, 1H,  $\text{CHH}$ ,  $^2\text{J} = 14.1$  Hz,  $^3\text{J} = 7.8$  Hz).  $^{13}\text{C}$  NMR ( $\text{D}_2\text{O}$ , 298 K)  $\delta$  40.59 ( $\text{CH}_2$ ), 57.47 ( $\text{C}^2$ ), 129.94 ( $\text{C}^7$ ), 131.56 ( $\text{C}^5$ ,  $\text{C}^5'$ ), 132.11 ( $\text{C}^6$ ,  $\text{C}^6'$ ), 139.18 ( $\text{C}^4$ ), 183.88 ( $\text{C}^1$ ). [ $\text{Zn}(\text{S-Ala})_2(\text{H}_2\text{O})$ ] (**2b**):  $^1\text{H}$  NMR ( $\text{D}_2\text{O}$ , 298 K),  $\delta$ , ppm: 3.62 (dd, 1H,  $\text{CH}_3\text{CH}$ ,  $^2\text{J} = 13.6$  Hz,  $^3\text{J} = 6.9$  Hz), 1.40 (d, 3H,  $\text{CH}_3\text{CH}$ ).  $^{13}\text{C}$  NMR ( $\text{D}_2\text{O}$ , 298 K)  $\delta$  20.52 ( $\text{CH}_3$ ), 52.35 ( $\text{C}^2$ ), 182.53 ( $\text{C}^1$ ).

#### 4. Conclusions

The composites based on chelate complexes of transition metals  $\text{Cu}(\text{S-Ala})_2$ -[ $\text{Cu}(\text{S-Phe})_2$ ] and [ $\text{Zn}(\text{S-Ala})_2(\text{H}_2\text{O})$ ]-[ $\text{Zn}(\text{S-Phe})_2(\text{H}_2\text{O})$ ] studied in this work and used in the EVS as chiral selectors are stable under experimental conditions and provide greater enantioselectivity compared to amino acids and complexes **1,2a,b** in the determination of chiral analytes such as Nap and Prp.

It has been shown that enantioselectivity depends on the complex-forming metal and on the composite structure. The best results are observed with copper complexes that have nearly planar structures. In general, it can be noted that sensors modified with various amino acid complexes of transition metals possess cross sensitivity [27] to enantiomers of biologically active compounds and can be used for constructing novel chiral multi-sensor platforms [14–16] in the future.

**Supplementary Materials:** The following supporting information can be downloaded at: <https://www.mdpi.com/article/10.3390/inorganics10080117/s1>. ESI-MS, QM for composite [ $\text{Cu}(\text{S-Ala})_2$ ]-[ $\text{Cu}(\text{S-Phe})_2$ ] (**1**) and [ $\text{Zn}(\text{S-Ala})_2(\text{H}_2\text{O})$ ]-[ $\text{Zn}(\text{S-Phe})_2(\text{H}_2\text{O})$ ] (**2**) and the structure data for complexes [ $\text{Cu}(\text{S-Phe})_2$ ] (**1a**), [ $\text{Zn}(\text{S-Phe})_2(\text{H}_2\text{O})$ ] (**2a**), [ $\text{Cu}(\text{S-Ala})_2$ ] (**1b**), [ $\text{Zn}(\text{S-Ala})_2(\text{H}_2\text{O})$ ] (**2b**).

**Author Contributions:** This work is a collaborative development of all the authors. R.A.Z.: development and research of enantioselective voltammetric sensors for the recognition of naproxen and propranolol enantiomers, conceptualization, methodology, and writing—original draft preparation. T.V.B.: synthesis and characterization of the [ $\text{Cu}(\text{S-Ala})_2$ ], [ $\text{Cu}(\text{S-Phe})_2$ ], [ $\text{Zn}(\text{S-Ala})_2(\text{H}_2\text{O})$ ], and [ $\text{Zn}(\text{S-Phe})_2(\text{H}_2\text{O})$ ]; conceptualization, methodology, and writing—original draft preparation. R.R.G., Y.B.T., M.N.G., and E.O.B.: software, validation, formal analysis, investigation. All authors have read and agreed to the published version of the manuscript.

**Funding:** This research received no external funding.

**Informed Consent Statement:** Consent was obtained from all study participants.

**Conflicts of Interest:** The authors declare no conflict of interests.

## References

1. Zor, E.; Bingol, H.; Ersoz, M. Chiral sensors. *Trends Anal. Chem.* **2019**, *121*, 115662. [[CrossRef](#)]
2. Zhu, G.; Kingsford, O.J.; Yi, Y.; Wong, K.-Y. Review—Recent Advances in Electrochemical Chiral Recognition. *J. Electrochem. Soc.* **2019**, *166*, H205–H217. [[CrossRef](#)]
3. Maistrenko, V.N.; Zil'berg, R.A. Enantioselective Voltammetric Sensors on the Basis of Chiral Materials. *J. Anal. Chem.* **2020**, *75*, 1514–1526. [[CrossRef](#)]
4. Niu, X.; Yang, X.; Li, H.; Liu, J.; Liu, Z.; Wang, K. Application of chiral materials in electrochemical sensors. *Microchim. Acta* **2020**, *187*, 1–18. [[CrossRef](#)] [[PubMed](#)]
5. Maistrenko, V.N.; Sidel'nikov, A.V.; Zil'berg, R.A. Enantioselective Voltammetric Sensors: New Solutions. *J. Anal. Chem.* **2018**, *73*, 1–9. [[CrossRef](#)]
6. Nguyen, L.A.; He, H.; Pham-Huy, C. Chiral drugs: An overview. *Int. J. Biomed. Sci.* **2006**, *2*, 85–100.
7. Hancu, G.; Modroiu, A. Chiral Switch: Between Therapeutical Benefit and Marketing Strategy. *Pharmaceuticals* **2022**, *15*, 240. [[CrossRef](#)]
8. Moein, M.M. Advancements of chiral molecularly imprinted polymers in separation and sensor fields: A review of the last decade. *Talanta* **2021**, *224*, 121794. [[CrossRef](#)]
9. BelBruno, J.J. Molecularly imprinted polymers. *Chem. Rev.* **2019**, *119*, 94–119. [[CrossRef](#)]
10. Radi, A.-E.; Wahdan, T.; El-Basiony, A. Electrochemical sensors based on molecularly imprinted polymers for pharmaceuticals analysis. *Cur. Anal. Chem.* **2019**, *15*, 219–239. [[CrossRef](#)]
11. Assavapanumat, S.; Yuthalekha, T.; Garrigue, P.; Goudeau, B.; Lapeyre, V.; Perro, A.; Sojic, N.; Wattanakit, C.; Kuhn, A. Potential induced fine-tuning the enantioaffinity of chiral metal phases. *Angew. Chem. Int. Ed.* **2019**, *58*, 3471–3475. [[CrossRef](#)] [[PubMed](#)]
12. Niu, X.; Yang, X.; Mo, Z.; Pan, Z.; Liu, Z.; Shuai, C.; Gao, Q.; Liu, N.; Guo, R. Electrochemical chiral recognition at molecular imprinting Au surfaces. *J. Electrochem. Soc.* **2019**, *166*, B1126–B1130. [[CrossRef](#)]
13. Assavapanumat, S.; Ketkaew, M.; Kuhn, A.; Wattanakit, C. Synthesis, characterization, and electrochemical applications of chiral imprinted mesoporous Ni surfaces. *J. Am. Chem. Soc.* **2019**, *141*, 18870–18876. [[CrossRef](#)] [[PubMed](#)]
14. Zilberg, R.A.; Maistrenko, V.N.; Kabirova, L.R.; Dubrovsky, D.I. Selective voltammetric sensors based on composites of chitosan polyelectrolyte complexes with cyclodextrins for the recognition and determination of atenolol enantiomers. *Anal. Methods* **2018**, *10*, 1886–1894. [[CrossRef](#)]
15. Zilberg, R.A.; Sidelnikov, A.V.; Maistrenko, V.N.; Yarkaeva, Y.A.; Khamitov, E.M.; Maksutova, E.I.; Kornilov, V.M. A Voltammetric Sensory System for Recognition of Propranolol Enantiomers Based on Glassy Carbon Electrodes Modified by Polyarylenephthalide Composites of Melamine and Cyanuric Acid. *Electroanalysis* **2018**, *30*, 619–625. [[CrossRef](#)]
16. Zil'berg, R.A.; Maistrenko, V.N.; Yarkaeva, Y.A.; Dubrovskii, D.I. An Enantioselective Voltammetric Sensor System Based on Glassy Carbon Electrodes Modified by Polyarylenephthalide Composites with  $\alpha$ -,  $\beta$ -, and  $\gamma$ -Cyclodextrins for Recognizing D- and L-Tryptophans. *J. Anal. Chem.* **2019**, *74*, 1245–1255. [[CrossRef](#)]
17. Zil'berg, R.A.; Zagitova, L.R.; Vakulin, I.V.; Yarkaeva, Y.A.; Teres, U.B.; Berestova, T.V. Enantioselective Voltammetric Sensors Based on Amino Acid Complexes of Cu(II), Co(III), and Zn(II). *J. Anal. Chem.* **2021**, *76*, 1438–1448. [[CrossRef](#)]
18. Yarkaeva, Y.A.; Dubrovskii, D.I.; Zil'berg, R.A.; Maistrenko, V.N.; Kornilov, V.M. A Voltammetric Sensor Based on a 3,4,9,10-Perylenetetracarboxylic Acid Composite for the Recognition and Determination of Tyrosine Enantiomers. *J. Anal. Chem.* **2020**, *75*, 1537–1545. [[CrossRef](#)]
19. Du, Y.; Mo, Z.; Wang, J.; Shuai, C.; Pei, H.; Chen, Y.; Yue, R. A novel chiral carbon nanocomposite based on cellulose gum modifying chiral tri-electrode system for the enantio-recognition of tryptophan. *J. Electroanal. Chem.* **2021**, *895*, 115390. [[CrossRef](#)]
20. Atta, N.F.; Galal, A.; Ahmed, Y.M. Highly conductive crown ether/ionic liquid crystal-carbon nanotubes composite based electrochemical sensor for chiral recognition of tyrosine enantiomers. *J. Electrochem. Soc.* **2019**, *166*, B623–B630. [[CrossRef](#)]
21. Niu, X.; Yang, X.; Li, H.; Shi, Q.; Wang, K. Chiral voltammetric sensor for tryptophan enantiomers by using a self-assembled multiwalled carbon nanotubes/ polyaniline/sodium alginate composite. *Chirality* **2021**, *33*, 248–260. [[CrossRef](#)] [[PubMed](#)]
22. Zil'berg, R.A.; Maistrenko, V.N.; Zagitova, L.R.; Guskov, V.Y.; Dubrovsky, D.I. Chiral voltammetric sensor for warfarin enantiomers based on carbon black paste electrode modified by 3,4,9,10-perylenetetracarboxylic acid. *J. Electroanal. Chem.* **2020**, *861*, 113986. [[CrossRef](#)]
23. Zagitova, L.R.; Maistrenko, V.N.; Yarkaeva, Y.A.; Zil'berg, R.A.; Zagitov, V.V.; Kovyazin, P.V.; Parfenova, L.V. Novel chiral voltammetric sensor for tryptophan enantiomers based on 3-neomenthylindene as recognition element. *J. Electroanal. Chem.* **2021**, *880*, 114939. [[CrossRef](#)]
24. Yarkaeva, Y.A.; Islamuratova, E.N.; Zagitova, L.R.; Guskov, V.Y.; Zil'berg, R.A.; Maistrenko, V.N. A Sensor for the Recognition and Determination of Tryptophan Enantiomers Based on Carbon-Paste Electrode Modified by Enantiomorphic Crystals of Bromotriphenylmethane. *J. Anal. Chem.* **2021**, *76*, 1345–1354. [[CrossRef](#)]
25. Upadhyay, S.S.; Kalambate, P.K.; Srivastava, A.K. Enantioselective biomimetic sensor for discrimination of R and S-Clopidogrel promoted by  $\beta$ -cyclodextrin complexes employing graphene and platinum nanoparticle modified carbon paste electrode. *J. Electroanal. Chem.* **2019**, *840*, 305–312. [[CrossRef](#)]
26. Mucoz, A.; González-Campo, M.; Riba-Moliner, M.; Baeza, M.; Mas-Torrent, M. Chiral magnetic-nanobiofluids for rapid electrochemical screening of enantiomers at a magneto nanocomposite graphene-paste electrode. *Biosens. Bioelectron.* **2018**, *105*, 95–102. [[CrossRef](#)]

27. Yarkaeva, Y.A.; Maistrenko, V.N.; Zagitova, L.R.; Nazyrov, M.I.; Berestova, T.V. Voltammetric sensor system based on Cu(II) and Zn(II) amino acid complexes for recognition and determination of atenolol enantiomers. *J. Electroanal. Chem.* **2021**, *903*, 115839. [[CrossRef](#)]
28. Zilberg, R.A.; Teres, Y.B.; Zagitova, L.R.; Yarkaeva, Y.A.; Berestova, T.V. Voltammetric sensor based on the copper (II) amino acid complex for the determination of tryptophan enantiomers. *Anal. Control.* **2021**, *25*, 193–204. [[CrossRef](#)]
29. Dybtsev, D.N.; Samsonenko, D.G.; Fedin, V.P. Porous coordination polymers based on carboxylate complexes of 3d metals. *Russ. J. Coord Chem.* **2016**, *42*, 557–573. [[CrossRef](#)]
30. Guk, D.A.; Krasnovskaya, O.O.; Beloglazkina, E.K. Coordination compounds of biogenic metals as cytotoxic agents in cancer therapy. *Russ. Chem. Rev.* **2021**, *90*, 1566. [[CrossRef](#)]
31. Berestova, T.V.; Khursan, S.L.; Mustafin, A.G. Experimental and theoretical substantiation of differences of geometric isomers of copper(II)  $\alpha$ -amino acid chelates in ATR-FTIR spectra. *Spectrochim. Acta A.* **2020**, *229*, 117950. [[CrossRef](#)]
32. Berestova, T.V.; Gizatov, R.R.; Galimov, M.N.; Mustafin, A.G. ATR-FTIR spectroscopic investigation of the cis- and trans-bis-( $\alpha$ -amino acids) copper(II) complexes. *J. Mol. Struct.* **2021**, *1236*, 130303. [[CrossRef](#)]
33. Dijkstr, A. The crystal structure of the copper complex of L-alanine. *Acta Cryst.* **1966**, *20*, 588–590. [[CrossRef](#)]
34. Helm, V.D.V.; Lawson, M.B.; Enwall, E.L. The Crystal Structure of Bis-(L-phenylalaninato)copper(II). *Acta Cryst.* **1971**, *27*, 2411–2418. [[CrossRef](#)]
35. Rombach, M.; Gelinsky, M.; Vahrenkamp, H. Coordination modes of aminoacids to zinc. *Inorg. Chim. Acta* **2002**, *334*, 25–33. [[CrossRef](#)]
36. Dalosto, S.D.; Ferreyra, M.G.; Calvo, R.; Piro, O.E.; Castellano, E.E. Structure of bis(L-alaninato)zinc(II) and single crystal EPR spectra of Cu(II) impurities. *J. Inorg. Biochem.* **1999**, *73*, 151–155. [[CrossRef](#)]
37. Markovic, M.; Judas, N. Sabolovic, Combined experimental and computational study of cis-trans isomerism in bis(L-valinato)copper(II). *J. Inorg. Chem.* **2011**, *50*, 3632–3644. [[CrossRef](#)]
38. Berestova, T.V.; Nosenko, K.N.; Lusina, O.V.; Kuzina, L.G.; Kulish, E.I.; Mustafin, A.G. Estimating the stability of metal-ligand bonding in carboxyl-containing polymer complexes by IR spectroscopy. *J. Struct. Chem.* **2020**, *61*, 1876–1887. [[CrossRef](#)]
39. Zhao, Y.; Truhlar, D.G. The M06 suite of density functionals for main group thermochemistry, thermochemical kinetics, noncovalent interactions, excited states, and transition elements: Two new functionals and systematic testing of four M06-class functionals and 12 other functional. *J. Theor. Chem. Acc.* **2008**, *120*, 215–241. [[CrossRef](#)]
40. Montes, R.H.O.; Stefano, J.S.; Richter, E.M.; Munoz, R.A.A. Exploring Multiwalled Carbon Nanotubes for Naproxen Detection. *Electroanalysis* **2014**, *26*, 1449–1453. [[CrossRef](#)]
41. Chunzhi, X.; Qiao, X.; Juanjuan, Q.; Qinghong, W.; Xia, L.; Yingzi, F. A biosensing interface based on Au@BSA nanocomposite for chiral recognition of propranolol. *Anal. Methods* **2016**, *8*, 3564–3569. [[CrossRef](#)]
42. Ebrahimi, S.; Afkhami, A.; Madrakian, T. Target -responsive host-guest binding-driven dual-sensing readout for enhanced electrochemical chiral analysis. *Analyst.* **2021**, *146*, 4865–4872. [[CrossRef](#)] [[PubMed](#)]
43. Jafari, M.; Tashkhourian, J.; Absalan, G. Electrochemical Sensor for Enantioselective Recognition of Naproxen Using LCysteine/Reduced Graphene Oxide Modified Glassy Carbon Electrode. *Anal. Bioanal. Chem. Res.* **2020**, *7*, 1–15.
44. Afkhami, A.; Kafrahi, F.; Ahmadi, M.; Madrakian, T. A new chiral electrochemical sensor for the enantioselective recognition of naproxen enantiomers using l-cysteine self-assembled over gold nanoparticles on a gold electrode. *RSC Adv.* **2015**, *5*, 58609–58615. [[CrossRef](#)]
45. Guo, L.; Huang, Y.; Zhang, Q.; Chen, C.; Guo, D.; Chen, Y.; Fu, Y. Electrochemical Sensing for Naproxen Enantiomers Using Biofunctionalized Reduced Graphene Oxide Nanosheets. *J. Electrochem. Soc.* **2014**, *161*, B70–B74. [[CrossRef](#)]
46. Santos, S.X.; Cavalheiro, E.T.G.; Brett, C.M.A. Analytical Potentialities of Carbon Nanotube/Silicone Rubber Composite Electrodes: Determination of Propranolol. *Electroanalysis* **2010**, *22*, 2776–2783. [[CrossRef](#)]
47. Diele, A.G.A.; Pradela-Filho, L.A.; Santos, A.L.R.; Faria, A.M.; Takeuchi, R.M.; Karimi-Malehc, H.; Santos, A.L. Uncured Polydimethylsiloxane as Binder Agent for Carbon Paste Electrodes: Application to the Quantification of Propranolol. *J. Braz. Chem. Soc.* **2019**, *30*, 1988–1998. [[CrossRef](#)]
48. Zilberg, R.A.; Yarkaeva, Y.A.; Provorova, Y.R.; Gus'kov, V.Y.; Maistrenko, V.N. Voltammetric determination of propranolol enantiomers in the model solutions of pharmaceutical forms and biological fluids. *Anal. Control.* **2018**, *22*, 292–302. [[CrossRef](#)]
49. Bin, L.; Huiting, L.; Lu, C.; Xiaofeng, W.; Xiangying, S. Differential potential ratiometric sensing platform for enantiorecognition of chiral drugs. *Anal. Biochem.* **2019**, *574*, 39–45. [[CrossRef](#)]
50. Wong, A.; Santos, A.M.; Silva, T.A.; Fatibello-Filho, O. Simultaneous determination of isoproterenol, acetaminophen, folic acid, propranolol and caffeine using a sensor platform based on carbon black, graphene oxide, copper nanoparticles and PEDOT:PSS. *Talanta* **2018**, *183*, 329–338. [[CrossRef](#)]
51. Santos, A.M.; Wong, A.; Fatibello-Filho, O. Simultaneous determination of salbutamol and propranolol in biological fluid samples using an electrochemical sensor based on functionalized-graphene, ionic liquid and silver nanoparticles. *J. Electroanal. Chem.* **2018**, *824*, 1–8. [[CrossRef](#)]
52. Zhang, Q.; Guo, L.; Huang, Y.; Chen, Y.; Guo, D.; Chen, C.; Fu, Y. An electrochemical chiral sensing platform for propranolol enantiomers based on size-controlled gold nanocomposite. *Sensor. Actuator. B.* **2014**, *199*, 239–246. [[CrossRef](#)]
53. McLean, A.D.; Chandler, G.S. Contracted Gaussian-basis sets for molecular calculations. 1.2nd row atoms, Z=11-18. *J. Chem. Phys.* **1980**, *72*, 5639–5648. [[CrossRef](#)]

54. Raghavachari, K.; Binkley, J.S.; Seeger, R.; Pople, J.A. Self-Consistent Molecular Orbital Methods. 20. Basis set for correlated wave-functions. *J. Chem. Phys.* **1980**, *72*, 650–654. [[CrossRef](#)]
55. Wachters, A.J.H. Gaussian basis set for molecular wavefunctions containing third-row atoms. *J. Chem. Phys.* **1970**, *52*, 1033–1036. [[CrossRef](#)]
56. Hay, P.J. Gaussian basis sets for molecular calculations—Representation of 3D orbitals in transition-metal atoms. *J. Chem. Phys.* **1977**, *66*, 4377–4384. [[CrossRef](#)]
57. Raghavachari, K.; Trucks, G.W. Highly correlated systems: Excitation energies of first row transition metals Sc-Cu. *J. Chem. Phys.* **1989**, *91*, 1062–1065. [[CrossRef](#)]
58. Frisch, M.J.; Trucks, G.W.; Schlegel, H.B.; Scuseria, G.E.; Robb, M.A.; Cheeseman, J.R.; Scalmani, G.; Barone, V. *Gaussian 09*; Revision D.01; Gaussian, Inc.: Wallingford, CT, USA. Available online: <https://gaussian.com/g09citation> (accessed on 1 June 2022).
59. Adrienko, G.A. Chemcraft—Graphical Software for Visualization of Quantum Chemistry Computations. Available online: <https://www.chemcraftprog.com> (accessed on 15 June 2022).